Development of a Built-In Micro-Laser Doppler Velocimeter

Nobutomo Morita, Hirofumi Nogami, Eiji Higurashi, Takahiro Ito, and Renshi Sawada

***Abstract*— Our research group previously developed an integrated micro-laser Doppler velocimeter only 2.8 × 2.8 mm in area and 1-mm thick by minimizing a number of components with multifunctional parts, such as a glass cover with lenses for hermetic sealing and laser collimation, a silicon base for casing, a mirror mount, a laser diode bench, and others. In this paper, by applying a fast Fourier transform analysis to the sensor output, we successfully measured the velocities of plastic, paper, and aluminum objects over a wide velocity range, from 10 μm/s to 10 mm/s, within a 3.3% measurement error, without attaching any scale to the measurement target. We also verified feasible measurement distances for each object and examined how tilt installation error affected the measurements. [2015-0111]**

***Index Terms*— Laser Doppler velocimetry, micro optical sensor, velocity sensor.**

I. Introduction

MANY APPLICATIONS require measurements of the velocities of objects without contacting measurement targets. Velocity measurement devices are ideally extremely compact so they can be embedded into narrow spaces or high-speed movable parts, meeting recent needs for highly-integrated, highly-functional manufacturing equipment. Examples of applications include film feeding velocity monitoring by embedding such a device onto film manufacturing/processing equipment, slip control when grasping objects by embedding one into a robotic hand and having it deliver feedback on slip velocity, and fluid flow velocity measurements by embedding one onto a pipe wall.

There are three methods to measure velocity without contact: 1) optical flow, 2) optical linear encoder, and 3) laser Doppler velocimetry. Optical flow is a method of utilizing image processing to observe the motion of objects using cameras and computing [1], [2]. The system can measure the velocity of various parts individually: for example, the velocities of many cells [3], [4], and the motions of different body parts [5], [6]. However, visual learning must be performed before measurements are made, and in fact, these methods cannot be applied for low-contrast objects. They also tend to be expensive and bulky because a high–speed, high-resolution camera is required. An optical linear encoder can measure the velocity of an object using reflected light from a grating scale attached to the object. While the sensor can achieve high measurement accuracy, careful and accurate positioning of the grating scale is critical to its success. This is where laser Doppler velocimetry shines: it permits the measurement of velocity without additional attachments to the object, and the alignment requirements for the sensor and the object are less strict than those of encoders [7]. Sensors that employ it, called laser Doppler velocimeters (LDVs), can measure the velocity of any material that by itself or by its constituent particles—bubbles, cells, emulsion phases, etc.—can scatter irradiated light. Examples include solids like aluminum and cardboard or fluids like water, oil, and air. LDVs can make such measurements with high spatial resolution and without contact. These advantages have spurred the use of LDVs in many applications: for example, in paper manufacturing processes for controlling reel speed, in roll forming processes of steel for controlling steel feeding velocity [8], in fluid dynamics for observing complex flows [9]–[14], and in biomedicine for measuring blood flow [15]–[18].

However, the optical probe sizes of commercial LDVs range from several to tens of square centimeters because they require a number of optical components, such as a laser source, a photo-detector, a beam splitter, mirrors, and lenses. The sizes and weights of commercial LDVs make them difficult to be embedded into narrow spaces and high-speed movable parts. A smaller LDV has been developed that uses an integrated laser diode (LD) and photo diode (PD) 9 mm in diameter and 6 mm in height [19]. However, the total optical probe size including lenses is over several centimeters. There are no few-millimeter-sized LDVs including all the optical components mentioned above. These optical components also need to be aligned with high accuracy and the costs of LDVs are high. There is thus a need for a novel LDV fabricated by a new process that can greatly reduce device size and achieve greater productivity gains for the aforementioned applications. In our previous studies, we successfully developed integrated optical microsensors [20]–[24], including a few-millimeter-sized LDV sensor [25], by using photolithography fabrication techniques and integration techniques: for example, surface planar integration with highly accurate bonding [20] and 3-D structure formation by Si with cavities [25]. The sizes of these optical microsensors are only a few square millimeters. However, the LDV sensor we reported in [25] required its target object to be grating scale in order to obtain clear

Manuscript received April 26, 2015; revised January 2, 2016; accepted January 7, 2016. Date of publication February 3, 2016; date of current version March 31, 2016. Subject Editor C. Rembe.

N. Morita, H. Nogami, and R. Sawada are with Kyushu University, Fukuoka 819-0395, Japan (e-mail: morita@nano-micro.mech.kyushu-u.ac.jp; nogami@mech.kyushu-u.ac.jp; sawada@mech.kyushu-u.ac.jp).

E. Higurashi is with the University of Tokyo, 7-3-1 Hongo, Bunkyo-ku, Tokyo 113-8656, Japan (e-mail: eiji@su.t.u-tokyo.ac.jp).

T. Ito is with the Kyushu Institute of Technology, Iizuka 820-8502, Japan (e-mail: ito@mse.kyutech.ac.jp).

Color versions of one or more of the figures in this paper are available online at http://ieeexplore.ieee.org.

Digital Object Identifier 10.1109/JMEMS.2016.2518691

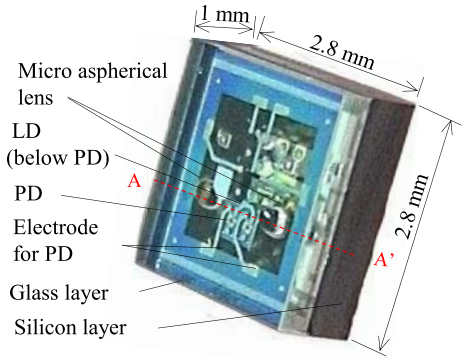

Fig. 1. Picture of the μ-LDV. The schematic of A-A′ section is shown in Fig. 3.

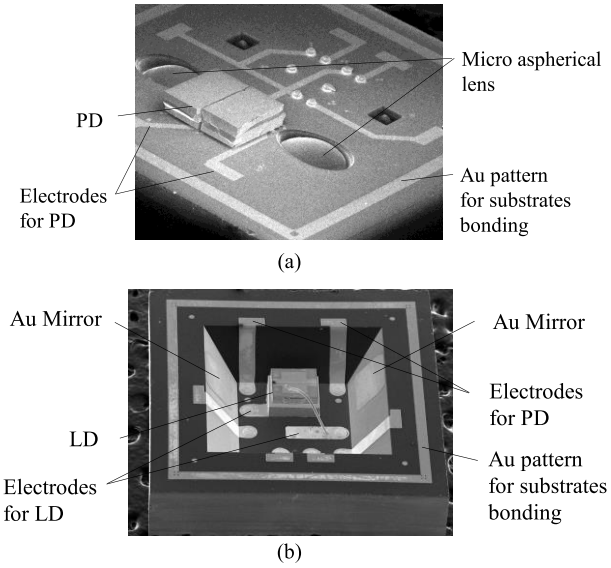

Fig. 2. SEM images of the components of the μ-LDV: (a) the glass substrate and (b) the Si substrate.

sine-waveform signals. The method allowed only a very narrow alignment error for the gap between the sensor chip and grating scale, which is too sensitive for industrial use. In contrast, general LDVs can measure scattering surfaces such as metal, plastic, or paper without any scale and without any contact, one of the strongest advantages of LDV measurement. Thus, few-millimeter-sized embeddable LDVs that can measure scattering surfaces are strongly desired for practical use.

In this research, we successfully used our highly integrated μ-LDV to measure the velocity of various scattering surfaces (aluminum, cardboard, and plastic) directly, without any attachment like a grating scale, by applying fast Fourier transform (FFT) analysis to the output of the device, and processing the resulting power spectra from the FFT analysis. We also confirmed characteristics of the measurement distance and tilt installation error corresponded to its allowable alignment error.

II. Micro-Laser Doppler Velocimeter

A. Design

Fig. 1 shows a picture of the μ-LDV. It consists of two elements, a pyrex glass substrate (Fig. 2(a)) and a Si substrate (Fig. 2(b)). Electrodes are formed on the back surface of the Pyrex glass substrate by depositing Au, and the InGaAs PIN PD (size: 280 × 460 × 150 μm; active diameter: 70 μm) is bonded onto the electrode. The electrode pad and light-receiving area of the PD are formed on the back surface. Micro aspherical lenses for collimating the laser can be formed by inductively coupled plasma (ICP) etching with a gray-scale-patterned photoresist structure [25], [26]. The Si substrate has a wet-etched cavity defined by (1 1 1) crystal planes [27], and this is used to build a free space and tilt surface for Au mirrors. Au mirrors and electrodes are formed on the cavity wall and cavity bottom by depositing Au. An edge-emitting distributed feedback laser diode (DFB-LD) chip (size: 400 × 450 × 100 μm; total output power: 5 mW; wavelength: 1.31 μm; wavelength stability: 0.1 nm/°C) was used to avoid using a beam splitter and to maintain the temperature stability of the wavelength. A DFB-LD was bonded onto the bottom of the Si cavity. The optical components are bonded by Au-Au surface-activated bonding [28], [29]. This method allows bonding in low-temperature conditions (150 °C), which is effective for preventing thermal damage to the LD and PD, and for precise alignment. Both substrates also can be bonded to become airtight by a bonding method using an Au pattern for substrate bonding (Fig. 2(a) and (b)). The electrodes on the Pyrex glass substrate are connected to electrodes on the Si substrate, and all electrodes are connected by through-hole electrodes from the sensor bottom to outside the sensor. This design enables the sensor to be fabricated with wafer-level packaging and to have an extremely small size (2.8 × 2.8 mm × 1.0 mm).

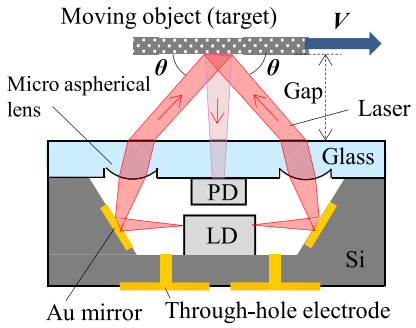

Fig. 3. Schematic of the μ-LDV along the A-A′ cross-section shown in Fig. 1.

B. Principle of Measurement

Fig. 3 shows a schematic of the A–A′ cross-section shown in Fig. 1. Two laser beams are simultaneously emitted from the LD, reflected by the Au mirrors, collimated by the refractive micro aspherical lenses, and impact the moving object. The moving object moves along a line orthogonal to the bisector of the two intersecting laser beams at velocity V. The two laser beams, which come from the left and right sides, are scattered by the moving object, and their frequencies are Doppler-shifted by Δf_L and Δf_R respectively:

$$\Delta f_L = -\frac{V}{\lambda} cos\theta \tag{1}$$

and

$$\Delta f_R = \frac{V}{\lambda} cos\theta, \tag{2}$$

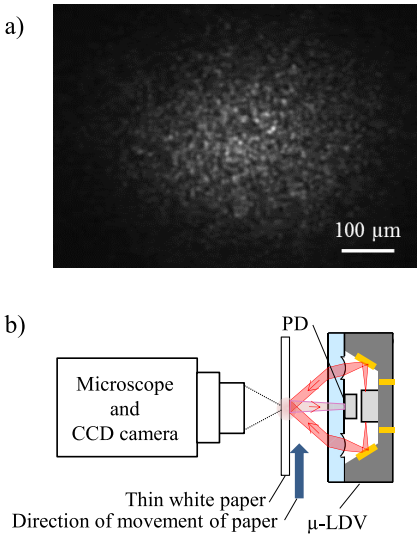

Fig. 4. (a) Speckle pattern of thin white paper. (b) Setup for the observation.

where θ ($= 66°$) is the angle between the direction of the laser beam and the direction of the object's motion, and λ is the wavelength of the laser. When those laser beams interfere, their Doppler-shifted frequency can be detected as the beat frequency by the PD, based on the principle of homodyne detection.

The beat frequency, f_d is equal to the difference in frequencies:

$$f_d = \left(f + \Delta f_R\right) - \left(f + \Delta f_L\right) = 2\frac{V}{\lambda} cos\theta. \tag{3}$$

In (3) [30], f_d is linearly proportional to V, and f is the initial laser beam frequency before it impacts the moving object. Although the frequency of a laser cannot be detected directly, as it is extremely high (230 THz for a wavelength of 1.31 μm) compared to the response speed of a PD, the PD can detect f_d because the beat frequency is significantly lower than the laser frequency f.

Fig. 4(a) shows an optical pattern of random dots, called a speckle pattern, formed by scattering light from two laser beams through a thin sheet of white paper parallel to a sensor surface, observed using the setup shown in Fig. 4(b). Note that we observed the transmitted speckle pattern on the opposite side of the paper from the PD, because it is difficult to make observations from the μ-LDV side due to space limitations. As the paper moves, each speckle dot moves in that direction and flickers with a beat frequency f_d related to the movement velocity. However, since each speckle dot flickers in mutually different phases, the total light intensity of the PD of the μ-LDV (sensitive area diameter: 70 μm) does not change greatly. To detect beat frequency from this slight change clearly and stably, we conducted a frequency analysis of the output signal using a FFT analyzer.

III. Experiments and Results

A. Experimental System

Fig. 5 shows a schematic of the experimental setup for measuring the μ-LDV characteristics for the velocities,

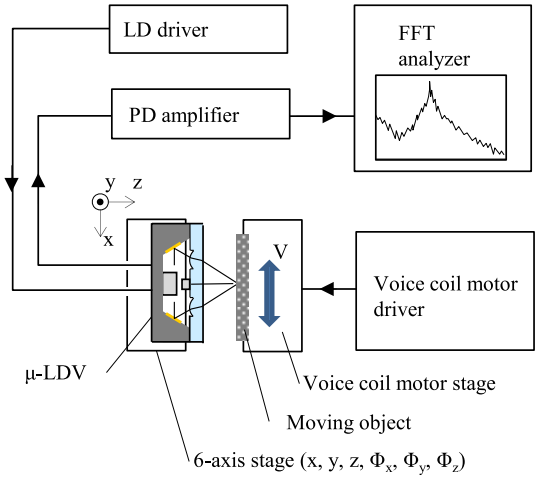

Fig. 5. Experimental setup.

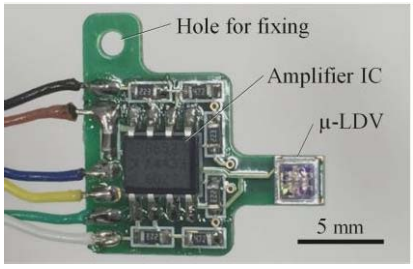

Fig. 6. Picture of the sensor head of the experimental system. The μ-LDV is mounted on a substrate with an amplifier circuit. The outline size is 16 × 16 × 2.5 mm.

Fig. 7. Images of the scattering boards used as moving objects. (a) Aluminum. (b) Cardboard. (c) Plastic.

materials, gap, and installation tilt errors of moving objects. To evaluate the characteristics of the μ-LDV, it is mounted on a substrate with an amplifier circuit, as shown in Fig. 6. The optical probe size including optical sensor chip and amplifier circuit is 16 × 16 × 2.5 mm, which is more than 100 times smaller than that of a commercial LDV. The μ-LDV was placed face-on to these moving objects with a 1.3-mm gap between the surfaces of the sensor and moving objects. We used three types of material as sample moving scattering objects: aluminum, cardboard, and black plastic, as shown in Fig. 7. These moving objects were attached to a voice coil motor to move them parallel to the x-axis of the sensor surface with a constant velocity. We set the sensor surface and moving object surface in parallel within a $\pm 1°$ tilt error for all axes. The LD driver supplied a current of 30 mA to the DFB-LD, whose wavelength stability with a change in temperature

TABLE I
THE SETTINGS FOR FFT AT EACH MEASUREMENT VELOCITY

Measurement velocity (μm/s)	FFT range (Hz)	Resolution bandwidth (Hz)	Resolution (μm/s)
10, 20	0 – 40	0.050	0.031
100	0 – 100	0.125	0.077
500	0 – 1,000	1.25	0.769
1,000, 2,000	0 – 2,000	2.50	1.538
3,000 - 10,000	0 – 10,000	12.5	7.686

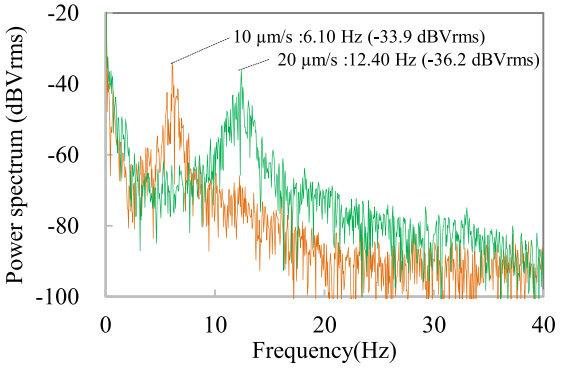

Fig. 8. Power spectra from aluminum at low velocities.

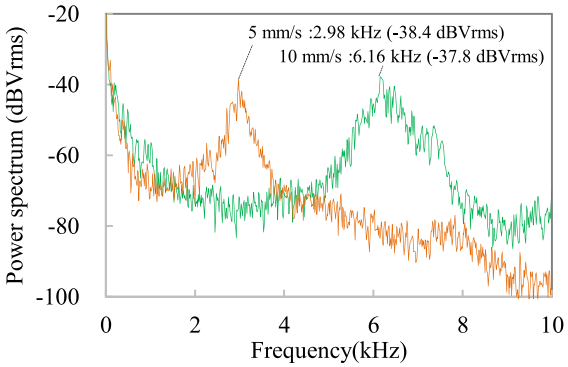

Fig. 9. Power spectra from aluminum at high velocities.

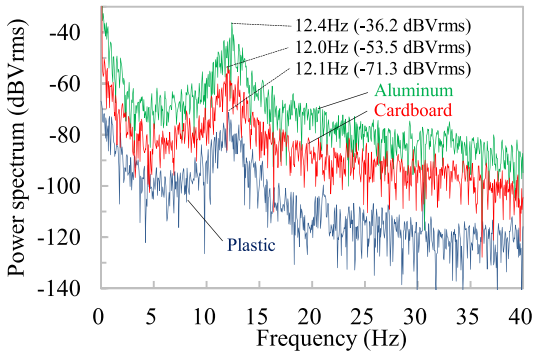

Fig. 10. Power spectra from three types of moving object material at a velocity of 20 μm/s.

is 0.1 nm/°C. The estimated error in the beat frequency with a change in wavelength with a 1 °C temperature difference is 0.08%. All measurements were performed at 25 ± 0.5 °C. The output power of each laser beam was 2.5 mW. The output voltage from the PD, generated from the scattered and Doppler-shifted laser light from the moving object, was amplified by the PD amplifier and transformed into a power spectrum form using a Fast Fourier Transform (FFT) analyzer.

B. Characteristics According to Velocity and Material

To determine the characteristics of the μ-LDV according to velocity and material, we performed an experiment with a wide range of velocities from 10 μm/s to 10,000 μm/s with aluminum, cardboard, and plastic scattering boards. The settings for FFT at each measurement velocity are shown in Table 1. Fig. 8 shows the power spectra obtained from aluminum at 10 μm/s and 20 μm/s. The power spectra were averaged over each ten measurements to obtain a smoother signal. Both power spectra have one clear peak each at different frequencies. These peak frequencies are the beat frequencies and are proportional to the velocities. Thus, the sensor can measure object velocities by reading the peak frequencies from power spectra. Fig. 9 shows the power spectra obtained from aluminum at 5,000 μm/s and 10,000 μm/s. In these results, clear peaks at different frequencies can also be seen. There are power differences of more than 20 dB between the peak and the noise in the spectrum, except in the lower 10% of the frequency range (lower velocity: 4 Hz; higher velocity: 1 kHz). Then, we defined the frequency at maximum power except in the lower 10% of the frequency range as the beat frequency.

In order to compare the effects of different surface characteristics of moving objects, we performed the same experiment with cardboard and plastic objects. Here, the PD output voltages in a static condition with aluminum, cardboard, and plastic were 1.62 V, 0.53 V, and 0.29 V, respectively. Fig. 10 shows example results comparing the power spectra obtained from the three types of scattering board at a velocity of 20 μm/s. The power spectra for each material differ substantially. However, the shapes of the power spectra are similar, and the peak frequencies cover a small range from 12.0 Hz to 12.4 Hz. Compared with the theoretical beat frequency of 12.3 Hz (at 20 μm/s), the maximum difference observed with the various experimental beat frequencies is 2.4% (cardboard). Fig. 11 shows power spectra obtained at a higher velocity, 10,000 μm/s. The shapes of the power spectra are also similar, and the peak frequencies range from 6.16 kHz to 6.35 kHz. The maximum difference between the theoretical beat frequency, 6.15 kHz (at 10,000 μm/s) and the various experimental beat frequencies is 3.3% (cardboard).

The beat frequencies for all measured velocities for each material and the theoretical beat frequencies expressed by (3) are plotted in Fig. 12. We observe good linearity between the object velocity and the measured beat frequency for all three material types. The measured results correspond to the theoretical beat frequencies over a wide range of velocities. The μ-LDV can measure the velocity of the targets even if the reflectance values of those targets are different. The power at each beat frequency is plotted in Fig. 13. These power values

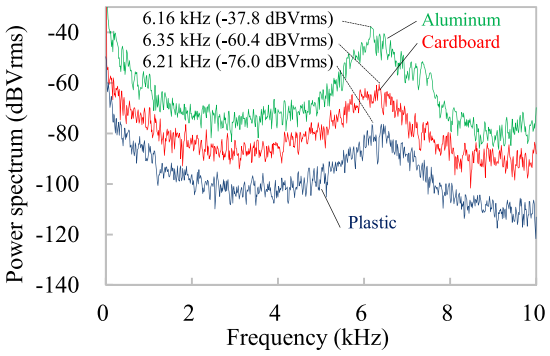

Fig. 11. Power spectra from three types of moving object material at a velocity of 10,000 μm/s.

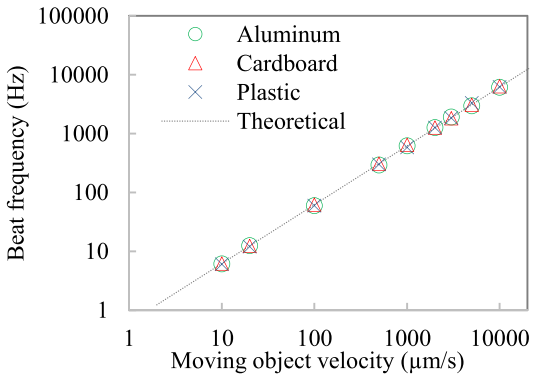

Fig. 12. Beat frequencies for all measured velocities and materials.

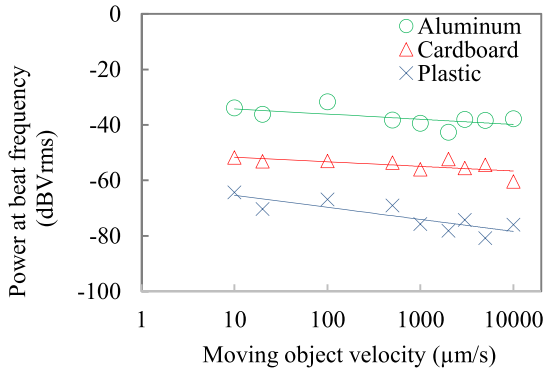

Fig. 13. Power at each beat frequency for all measured velocities and materials.

gradually decrease with increasing velocity: this divergence might be a problem for measurements at faster velocities, like on the other of tens of meters per second.

According to these findings, by reading the frequencies of the peaks of the power spectrum, the μ-LDV can measure the velocity of various objects, without requiring any information about the type of material and surface conditions.

C. Velocity Calculation Without FFT

All the reported data were converted from the time domain to the frequency domain using an FFT analyzer. The FFT analysis time interval T is inversely proportional to the frequency range, which is proportional to the frequency resolution. For example, the FFT analysis time interval was 80 ms for the measurements at a high velocity of 10,000 μm/s, shown in Fig. 11 (the FFT analyzer has a 10-kHz frequency range and a 12.5-Hz frequency resolution), or 20 s for the measurements at a low velocity of 20 μm/s, shown in Fig. 10 (with a 40-Hz frequency range and 0.05-Hz frequency resolution). The time interval required for FFT analysis may be a problem in cases that require a high response speed or a slow velocity (on the order of tens of micrometers per second or less). To solve this problem, we considered processing the signal in the time domain for real-time measurement. Fig. 14 shows the output voltage of the PD in the time domain for the measurement of the aluminum board moving at a velocity of 1 mm/s. We can observe the signal beating in the time domain, and the velocity of the moving aluminum board can be calculated by counting the number of times the signal crosses the average voltage, 38, over the elapsed, 30 ms. Thus, the calculated beat frequency and the velocity are 0.63 kHz and 1.02 mm/s, which are close to the results taken from power spectrum. Thus, this method can be used for velocity measurements in order to improve response speed and dynamic range if reduced measurement precision is allowable. This method may suffer from errors by miscounting the number of signal beats because the signal may not cross its average voltage as a result of fluctuation of DC voltage and variation of oscillation amplitude, and it is thus inferior to FFT analysis in terms of accuracy. On the other hand, FFT analysis requires a frequency range to be set appropriate to the velocity range of the measurement object. Using the crossing counting method at a higher sampling frequency, the sensor appears to achieve a high response time and a wide dynamic measurement range.

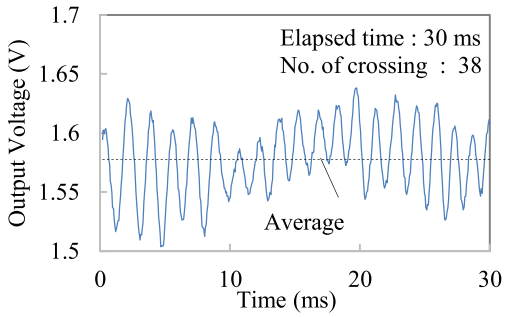

Fig. 14. Output voltage of the PD in the time domain for the measurement of the aluminum board moving at a velocity of 1 mm/s.

D. Characteristics for Measurement Distance

The available measurement distance is one of the most important factors in performance, and the desired specifications depend on its application. On the one hand, a smaller measurement volume is desired to obtain a high spatial resolution in the velocity measurement of fluids. On the other hand, in surface velocity measurements, a narrow but deep measurement volume is desired to avoid the measurement instability caused when the measurement volume miss measurement object as a result of surface roughness or vibration perpendicular to the measurement direction. We performed

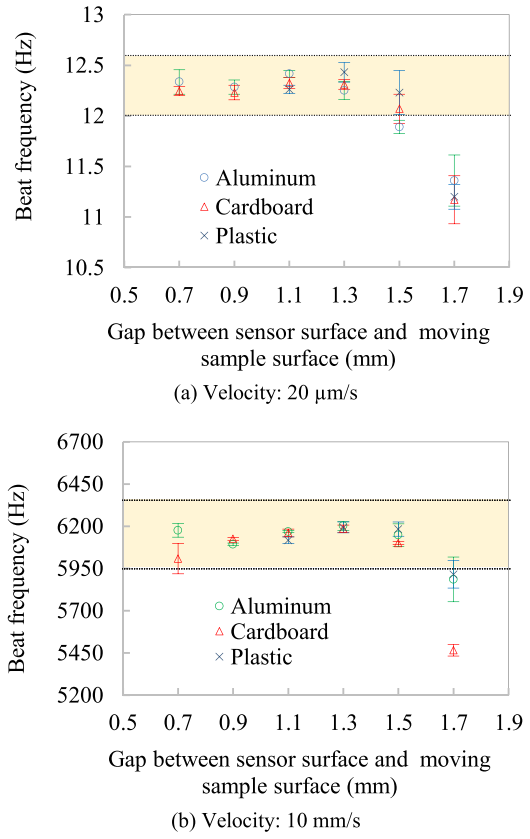

Fig. 15. Beat frequencies by changing measurement distance with three types of moving objects. The colored area indicates the allowable beat frequency range: (a) ±2.4% and (b) ±3.3% of the theoretical value.

velocity measurements at velocities of 20 μm/s and 10 mm/s while changing the measurement distance within the range that the μ-LDV displayed a beat frequency. In order to evaluate measurements stability, measurements were carried out 10 times under each set of conditions, and the mean value and standard deviation were calculated. Fig.15 (a) and (b) show the result. The colored area indicates the error range measured in Section III. B; ±2.4% of the theoretical beat frequency at 20 μm/s and ±3.3% of the theoretical beat frequency at 10 mm/s. We defined the distance range whose beat frequency fell within this error range as the measureable distance range. Outside the measurable distance ranges, beat frequencies had larger dispersion and tended to be lower than the corresponding theoretical beat frequencies, because the sharpness of the beat frequencies decreased, making the signal susceptible to noise. At the distances of 0.7 mm and 0.9 mm for the both velocities, it was impossible to detect any beat frequency for the plastic object. Looking at the data for both velocities by object surface material, the measurable distance ranges are from 0.7 mm to 1.5 mm (0.8 mm) for aluminum, from 0.9 mm to 1.3 mm (0.4 mm) for cardboard, and from 1.1 mm to 1.3 mm (0.2 mm) for plastic. We assume that the difference arises from differences in the intensity of the light reflected from each moving object. Although the measurable distance ranges differ between object surfaces, all measurable distance ranges are much wider than the range we previously reported for the affixed-grating method (i.e., 0.05 mm) [25].

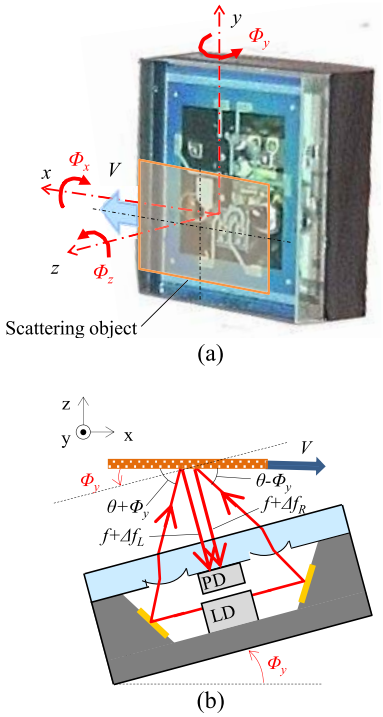

Fig. 16. Schematics of (a) installation tilt error and (b) the effects of tilt installation error around the y axis, Φ_y.

E. Characteristics for Tilt Installation Error

An estimation of the effect of installation error on the operation of a μ-LDV is a very important practice. We calculated the theoretical beat frequencies for tilt installation error around the x-, y-, and z-axes, as shown in Fig. 16(a). For a tilt installation error around the y-axis (Fig. 16(b)), the Doppler-shifted frequencies Δf_L and Δf_R in (1) and (1) are replaced, respectively, by:

$$\Delta f_L = -\frac{V}{\lambda} cos(\theta + \Phi_y) \tag{4}$$

and

$$\Delta f_R = \frac{V}{\lambda} cos(\theta - \Phi_y). \tag{5}$$

Then, the beat frequency for tilt installation error, $f_{d\Phi y}$ is:

$$f_{d\Phi_y} = 2\frac{V}{\lambda} cos\theta \cdot \cos \Phi_y. \tag{6}$$

The error around the z and x axes can be calculated in a similar way:

$$f_{d\Phi_z} = 2\frac{V}{\lambda} cos\theta \cdot \cos \Phi_z \tag{7}$$

and

$$f_{d\Phi_x} = 2\frac{V}{\lambda} cos\theta, \tag{8}$$

where $f_{d\Phi z}$ and $f_{d\Phi x}$ are the beat frequencies for tilt installation errors around the z and x axes, respectively.

In order to ensure that the μ-LDV operates in accordance with the theoretical equations (6–8), we performed an experiment for tilt installation error using the same set-up used previously. White hard cardboard was used as the moving object, owing to its flatter surface and high diffusivity.

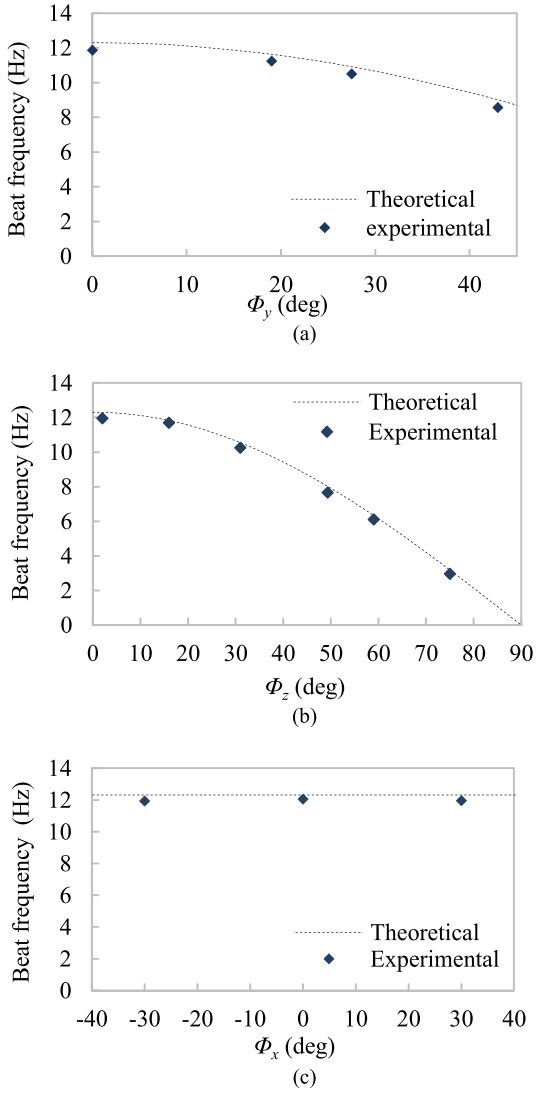

Fig. 17. Theoretical and experimental results for beat frequencies for tilt installation error around each axis at a velocity of 20 μm/s. (a) Around the y axis. (b) Around the z axis. (c) Around the x axis.

The velocity of the moving object was set at 20 μm/s. Fig. 17(a), (b), and (c) show the experimental results and theoretical beat frequencies for the errors Φ_y, Φ_z, and Φ_x, respectively. All the experimental data points lie along each theoretical line. According to results, tilt error around the x-axis has no discernible impact on beat frequency, and the μ-LDV measures the x component of the velocity, independently. Additionally, installation errors of Φ_y and Φ_z multiply the beat frequencies by cos Φ_y and cos Φ_z. Thus, when Φ is around 0, cos Φ is nearly 1 ($e.g.$, cos $5^\circ = 0.9962$), and the tilt error does not greatly affect the measurement. This useful characteristic is one of the advantages of an LDV measurement.

IV. Conclusion

In our previous research, we developed a micro-laser Doppler velocimeter (μ-LDV) only 2.8×2.8 mm in area and 1.0 mm in thickness, with a unique 3-D structure consisting of a Si substrate with cavities and a Pyrex glass substrate with micro aspherical lenses. Although its unique structure allowed the sensor to be incredibly small, it was limited in that it was only able to measure velocity of grating scale affixed to an object. In this paper, by applying FFT analysis to the output of the μ-LDV, and thereafter determining the frequency at the peak power of the power spectra resulting from this FFT analysis, we achieved velocity measurements ranging from 10 μm/s to 10,000 μm/s within 3.3 % measurement error for objects made of aluminum, cardboard, and plastic. We went on to examine the allowable measurement distances characteristic of these three materials, finding ranges of 0.8 mm for aluminum, 0.4 mm for cardboard, and 0.2 mm for plastic. These ranges are very wide when compared with the sensor thickness, and with our previously reported affixed-grating method (i.e., 0.05 mm). We also examined the effects of tilt installation error on the measured beat signal, and found they were small. While in this study, the glass substrate and the Si substrate were assembled after dicing the pieces individually, the design enables the μ-LDV to be fabricated with wafer-level packaging. This is effective not only for miniaturization, but also for reducing fabrication costs and enabling mass production. Although the accuracy of our LDV is not greater than that of commercial LDVs, the innovative small size, lightweight, and wide measurable distance range enable the sensor to be embedded into the narrow spaces and high-speed movable parts of complex mechanical systems, such as small multiaxial stages, manipulators, and robots, without high alignment accuracy. Embedding the μ-LDV into a robotic hand can realize a built-in slip sensor; embedding it into a pipe can realize a built-in flowmeter. The possibilities do not stop there: the small size, lightweight, its mass productive design, and applicability to a diverse range of materials are characteristics that our μ-LDV possesses that give it a utility advantage for velocimetry in various fields.

References

[1] C. L. Fennema and W. B. Thompson, "Velocity determination in scenes containing several moving objects," *Comput. Graph. Image Process.*, vol. 9, no. 4, pp. 301–315, 1979.
[2] B. K. P. Horn and B. G. Schunck, "Determining optical flow," *Artif. Intell.*, vol. 17, no. 13, pp. 185–203, 1981.
[3] D. Gerlich, J. Mattes, and R. Eils, "Quantitative motion analysis and visualization of cellular structures," *Methods*, vol. 29, no. 1, pp. 3–13, 2003.
[4] K. Miura, "Tracking movement in cell biology," *Microscopy Techn.*, vol. 95, pp. 267–295, May 2005.
[5] A. Yilmaz, O. Javed, and M. Shah, "Object tracking: A survey," *ACM Comput. Surv.*, vol. 38, no. 4, 2006, Art. ID 13.
[6] T. Brox and J. Malik, "Large displacement optical flow: Descriptor matching in variational motion estimation," *IEEE Trans. Pattern Anal. Mach. Intell.*, vol. 33, no. 3, pp. 500–513, Mar. 2011.
[7] Y. Yeh and H. Z. Cummins, "Localized fluid flow measurements with an He–Ne laser spectrometer," *Appl. Phys. Lett.*, vol. 4, no. 10, pp. 176–178, 1964.
[8] E. B. Li, A. K. Tieu, and W. Y. D. Yuen, "Measurements of velocity distributions in the deformation zone in cold rolling by a scanning LDV," *Opt. Lasers Eng.*, vol. 35, no. 1, pp. 41–49, 2001.
[9] R. J. Goldstei and W. F. Hagen, "Turbulent flow measurements utilizing the doppler shift of scattered laser radiation," *Phys. Fluids*, vol. 10, no. 6, pp. 1349–1354, 1967.
[10] H. J. Hussein, S. P. Capp, and W. K. George, "Velocity measurements in a high-Reynolds-number, momentum-conserving, axisymmetric, turbulent jet," *J. Fluid Mech.*, vol. 258, pp. 31–75, Jan. 1994.
[11] D. A. Lyn, S. Einav, W. Rodi, and J.-H. Park, "A laser-Doppler velocimetry study of ensemble-averaged characteristics of the turbulent near wake of a square cylinder," *J. Fluid Mech.*, vol. 304, pp. 285–319, Dec. 1995.

[12] S. M. Mousavian and A. F. Najafi, "Numerical simulations of gas–liquid–solid flows in a hydrocyclone separator," *Arch. Appl. Mech.*, vol. 79, pp. 395–409, May 2008.
[13] M. Sumida, T. Senoo, and J. Yamamoto, "LDV measurements of velocity distribution in unsteady bend flow," *Int. J. Mining Metall. Mech. Eng.*, vol. 2, no. 1, pp. 21–23, 2014.
[14] I. Drăghici, S. Muntean, A. I. Bosioc, and L. E. Anton, "LDV measurements of the velocity field on the inlet section of a pumped storage equipped with a symmetrical suction elbow for variable discharge values," in *Proc. IOP Conf. Ser., Earth Environ. Sci.*, vol. 22. 2014, p. 032017.
[15] C. E. Riva, G. T. Feke, B. Eberli, and V. Benary, "Bidirectional LDV system for absolute measurement of blood speed in retinal vessels," *Appl. Opt.*, vol. 18, no. 13, pp. 2301–2306, 1979.
[16] R. M. Werkmeister *et al.*, "Bidirectional Doppler Fourier-domain optical coherence tomography for measurement of absolute flow velocities in human retinal vessels," *Opt. Lett.*, vol. 33, no. 24, pp. 2967–2969, 2008.
[17] H. Nishihara, J. Koyama, N. Hoki, F. Kajiya, M. Hironaga, and M. Kano, "Optical-fiber laser Doppler velocimeter for high-resolution measurement of pulsatile blood flows," *Appl. Opt.*, vol. 21, no. 10, pp. 1785–1790, 1982.
[18] S. Akiguchi *et al.*, "Application of a micro-multipoint laser doppler velocimeter for *in vivo* evaluation of subcutaneous blood flow," *IEEJ Trans. Elect. Electron. Eng.*, vol. 8, no. 6, pp. 652–653, 2013.
[19] L. Scalise and N. Paone, "Laser Doppler vibrometry based on self-mixing effect," *Opt. Lasers Eng.*, vol. 38, nos. 3–4, pp. 173–184, 2002.
[20] R. Sawada, E. Higurashi, and T. Ito, "Highly accurate and quick bonding of a laser-diode chip onto a planar lightwave circuit," *Precis. Eng.*, vol. 25, no. 4, pp. 293–300, Oct. 2001.
[21] R. Sawada, E. Higurashi, and Y. Jin, "Hybrid microlaser encoder," *J. Lightw. Technol.*, vol. 21, no. 3, pp. 815–820, Mar. 2003.
[22] E. Higurashi, R. Sawada, and T. Ito, "An integrated laser blood flowmeter," *J. Lightw. Technol.*, vol. 21, no. 3, pp. 591–595, Mar. 2003.
[23] K. Nishihara *et al.*, "Development of a wireless sensor for the measurement of chicken blood flow using the laser Doppler blood flow meter technique," *IEEE Trans. Biomed. Eng.*, vol. 60, no. 6, pp. 1645–1653, Jun. 2013.
[24] N. Morita and R. Sawada, "Optical micro sensors integration and application," in *Proc. IEEE CPMT Symp. Jpn.*, Nov. 2014, pp. 3–6.
[25] E. Higurashi, D. Chino, T. Suga, and R. Sawada, "Au–Au surface-activated bonding and its application to optical microsensors with 3-D structure," *IEEE J. Sel. Topics Quantum Electron.*, vol. 15, no. 5, pp. 1500–1505, Sep./Oct. 2009.
[26] Y. Oppliger, P. Sixt, J. M. Stauffer, J. M. Mayor, P. Regnault, and G. Voirin, "One-step 3D shaping using a gray-tone mask for optical and microelectronic applications," *Microelectron. Eng.*, vol. 23, pp. 449–454, Jan. 1994.
[27] R. Chutani, N. Passilly, J. Albero, M. Baranski, and C. Gorecki, "Deep wet-etched silicon cavities for micro-optical sensors: Influence of masking on 111 sidewalls surface quality," *J. Microelectromech. Syst.*, vol. 23, no. 3, pp. 585–591, 2014.
[28] T. Suga, T. Itoh, Z. Xu, M. Tomita, and A. Yamauchi, "Surface activated bonding for new flip chip and bumpless interconnect systems," in *Proc. 52nd Electron. Compon. Technol. Conf.*, 2002, pp. 105–111.
[29] E. Higurashi, T. Imamura, T. Suga, and R. Sawada, "Low-temperature bonding of laser diode chips on silicon substrates using plasma activation of Au films," *IEEE Photon. Technol. Lett.*, vol. 19, no. 24, pp. 1994–1996, Dec. 15, 2007.
[30] J. B. Abbiss, T. W. Chubb, and E. R. Pike, "Laser Doppler anemometry," *Opt. Laser Technol.*, vol. 6, no. 6, pp. 249–261, 1974.

Nobutomo Morita received the B.E. and M.E. degrees from Kyushu University, Fukuoka, Japan, in 2010 and 2012, respectively, where he is currently pursuing the Ph.D. degree in engineering. His research interests include MEMS-based devices, focusing mainly on optical laser Doppler sensors.

Hirofumi Nogami received the B.E. degree from the Department of Mechanical Engineering, Kyushu University, in 2005, and the Ph.D. degree from the Graduate School of Systems Life Sciences, Kyushu University, in 2011. He was with the Research Center for Ubiquitous MEMS and Micro Engineering, National Institute of Advanced Industrial Science and Technology, as a Postdoctoral Researcher from 2011 to 2013. Since 2014, he has been an Assistant Professor with Kyushu University. His research works are potentially in commercial development in animal health monitoring system and the wireless sensor node. He was involved in research on optical blood flow sensor using MEMS technology.

Eiji Higurashi received the M.E. and Ph.D. degrees from Tohoku University, Sendai, Japan, in 1991 and 1999, respectively. He was with Nippon Telegraph and Telephone Corporation, Tokyo, Japan, from 1991 to 2003, where he was engaged in the field of laser manipulation and optical microsensors. He was an Associate Professor with the Research Center for Advanced Science and Technology, University of Tokyo, from 2004 to 2014. He is currently an Associate Professor with the Department of Precision Engineering, University of Tokyo. His current research interests include low-temperature bonding methods, and the integration and packaging of optical microsystems.

Takahiro Ito received the B.E. and M.E. degrees in mechanical engineering from the University of Tokyo, Japan, in 1983 and 1985, respectively; the M.S. degree in computer science from the University of Illinois at Urbana–Champaign in 1992; and the Ph.D. degree from the University of Tokyo in 2002. In 1985, he joined NTT Electrical Communication Laboratories, Tokyo. Since 2008, he has been a Professor with the Kyushu Institute of Technology, Japan. His research interests are micromechanism, sensor, and MEMS devices for medical application.

Renshi Sawada received the B.E., M.E., and Ph.D. degrees from Kyushu University, Fukuoka, Japan, in 1976, 1978, and 1995, respectively. In 1978, he joined Nippon Telegraph and Telephone Corporation, Tokyo, Japan, where he was engaged in research on the polishing of Si substrates, gettering of Si crystalline defects, fabrication of dielectrically isolated Si substrates (silicon on insulator substrate process), micromirror array, and integrated optical displacement sensors attachable to animals and humans for networking. Since 2004, he has been with Kyushu University. He was an Editor of the *Journal of Micromechanics and Microengineering*, and is also a Fellow of the Institute of Physics.